Interface Deformable, Thermally Sensitive Hydrogel-Elastomer Hybrid Fiber for Versatile Underwater Sensing

Chengmin Wang, Baohu Wu, Shengtong Sun, and Peiyi Wu**

C. Wang, Prof. S. Sun, Prof. P. Wu
State Key Laboratory for Modification of Chemical Fibers and Polymer Materials, College of Chemistry, Chemical Engineering and Biotechnology, Center for Advanced Low-dimension Materials, Donghua University, Shanghai 201620, China
E-mail: shengtongsun@dhu.edu.cn; wupeiyi@dhu.edu.cn

Dr. B. Wu
Jülich Centre for Neutron Science (JCNS) at Heinz Maier-Leibnitz Zentrum (MLZ) Forschungszentrum Jülich, Lichtenbergstr. 1, 85748 Garching, Germany

Keywords: underwater sensing, hydrogel fiber, stretchable photonics, bioinspiration

ABSTRACT: Underwater sensing plays a vital role in perceiving various hydrodynamic stimuli for underwater operations, while fishes evolve an adaptable, durable, and multifunctional lateral line sensory system to feel mechanical deformations from nearly all sources as well as water temperature changes. Such perfect integration of multiple functions into one biological system poses a great challenge for artificial soft sensors. Here we demonstrate, by constructing a stretchable and water-proof core-cladding hydrogel-elastomer hybrid optical fiber, nearly all the underwater sensations of fish lateral lines can be realized with unprecedented sensing stability. High-refractive-index salt, LiBr, is introduced to the hydrogel core to enable long-range light propagation with a low loss coefficient (~0.32 dB/cm), and the dissimilar yet tightly adhered hydrogel-elastomer interface is readily deformable, contributing to the ultrasensitive optical response to subtle environmental stimulations, induced by either motions, hydrostatic pressure variations, ultrasonic/audible sound waves, or water flows. Moreover, the optical loss of the hybrid fiber is linearly responsive to wide temperature changes (5-70 ^{o}C), caused by the altered light scattering from hydrogel chain clustering. The present elastomer-hydrogel hybrid optical fiber offers a new designing strategy in developing next-generation underwater stretchable ray-optic sensors.

Underwater sensing is extremely important for many underwater vehicles, robots, communication, and human diving operations in exploring the abundant mysteries and resources in the huge ocean. In nature, fishes have evolved a lateral line system to percept various hydrodynamic stimuli including minute water movements, pressure variations, water flows, acoustic waves, and to some degree, temperature, for the spatial awareness and the ability to navigate in the complex underwater environment (**Figure 1**).[1] With lateral line as the passive sensing system, blind cave fishes, for example, are capable to 'see' their surroundings even without eyes. Inspired by the structure and versatile sensing functionalities of lateral lines, people have developed a variety of underwater flow sensors based on either sensing arrays manufactured by microelectromechanical systems (MEMS)[2-4] or fiber optics by photonic modulation/fabrication techniques.[5, 6] Although these conventional miniaturized or fiber-like sensors have well mimicked the hydrodynamic sensitivity of fish lateral lines, they are generally based on hard materials that are not able to reconfigure autonomously in response to stress and surrounding changes.[7, 8] This leads to severe limitations for their integration with/at stretchable and biological interfaces caused by severely mismatched mechanical properties, especially in the boosted human-friendly wearable, implantable, and "Internet of Things" scenarios.

In recent years, the rapid development of soft electronics[9-14] and soft photonics[7, 15-17] provides more opportunities for underwater sensing. Comparing to soft electronic sensors that are vulnerable to electromagnetic and conductive medium interference, soft optical sensors based on the control of light-matter interactions show great advantages to conceive underwater sensing systems. In particular, at scales larger than light wavelength, the focusing of light via total internal reflection underlying light propagation in optical fibers represent one of the most effective ray-optic sensing types.[7] Transparent materials that are structurally functionalized, mechanically compliant, dynamically adaptive, sensitive to stimuli changes, and capable of homeostasis are ideal options for constituting ray-optic sensing systems. So far,

mainly two kinds of transparent materials have been exploited for fiber-based soft optics. Elastomers, like silicone,[18] polyurethane,[19] thermoplastic elastomers,[20, 21] biodegradable elastomers,[22] and liquid crystalline elastomers[23], were extensively used for optical fiber-based deformation and temperature sensing, imaging as well as actuating. However, most elastomers are inherently insensitive to environmental changes, and their Young's moduli are also much higher than water,[24, 25] leading them to be insufficient to detect very subtle hydrodynamic perturbations at underwater conditions. An alternative is transparent hydrogels with matching Young's moduli with biological tissues, excellent biocompatibility, widely adjustable mechanical properties and refractive indices as well as easy functionalization.[26-32] For instance, stretchable step-index optical fibers based on the core-cladding polyacrylamide/alginate hydrogels were successfully employed for multiplexed strain sensing,[28] continuous glucose monitoring[29] and chronic optogenetic brain modulation.[31] Nevertheless, although hydrogel optical fibers exhibit the unprecedented advantages of optical sensor flexibility and photoconductivity, bare hydrogel fibers are highly susceptible to the permeable masses in wet environment, which hinders their uses for durable underwater sensing of hydrodynamic changes as fishes do with the lateral line system.

Herein, by integrating the respective merits of elastomers and hydrogels, we propose a new strategy of well-defined, step-index elastomer-coated hydrogel optical fibers (ECHOFs) for versatile underwater optical sensing with ultrahigh stability. As shown in **Figure 1**, transparent polydimethylsiloxane (PDMS) with a lower refractive index is chosen as the elastomeric cladding, and soft yet highly stretchable polyacrylamide (PAAm) hydrogel as the core whose refractive index was significantly improved by the addition of a high-refractive-index salt (lithium bromide, LiBr). Such a hybrid core-cladding structure of ECHOF enables not only a low propagation loss along the fiber but also highly sensitive and durable sensing for a variety of underwater stimuli with unexpected stability, such as movements, hydrostatic

pressure, flow perturbations, acoustic waves, and temperature, which have never been realized by traditional soft electrical and optical sensors in an all-in-one sensing system.

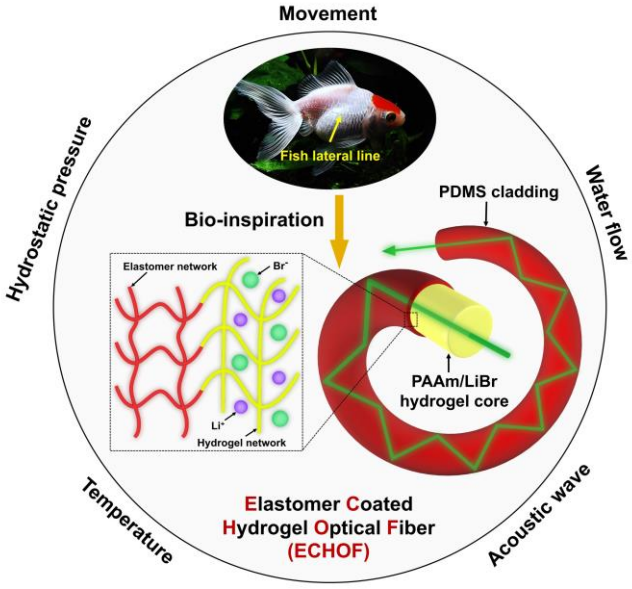

Figure 1. Schematic design for the core-cladding structure of ECHOF. The ECHOF consists of an ultrathin silicone cladding and LiBr-infiltrated PAAm hydrogel core, which allows for both stable and low-loss light propagation and multiple optical sensations via structural deformations or transformations, similar to the underwater sensory functions of fish lateral line system.

ECHOF was prepared by UV-induced polymerization of hydrogel precursor (AAm monomer, crosslinker, photo-initiator, LiBr) in a pre-formed PDMS hollow tube. We fabricated PDMS hollow tube with a typical outer diameter of 1 mm and ultrasmall thickness of ~30 μm via a sacrificial templating method, which can be made in 50 cm long with good uniformity and liquid encapsulating ability (Figure S1, S2, Movie S1). Subsequent hydrogel formation resulted in a well-defined core-cladding structure of ECHOF with high uniformity and pre-designed cross-section (**Figure 2**a, Figure S3). Notably, the robust adhesion between PDMS and PAAm hydrogel is critical for the structural integrity and synergetic deformation of ECHOF, which was achieved by a modified benzophenone strategy; wherein, benzophenone acts as a UV-assisted grafting agent for covalent crosslinking between dissimilar elastomer and hydrogel layers.[33, 34] Peeling test confirms the tight bonding between PAAm hydrogel core and PDMS cladding of ECHOF in comparison with hybrid PDMS/PAAm hydrogel fiber without benzophenone pre-treatment (Figure S4).

The total internal reflection (TIR) of light is essential for light propagation in an optical fiber, which refers to the phenomenon that all light is reflected back to the original medium when transmitted from an optically dense medium (high refractive index) to the interface of light thin medium (low refractive index). In terms of the relatively high refractive index of PDMS cladding (n = 1.413), only increasing the monomer concentration of PAAm hydrogel[28] is not sufficient to meet the TIR requirements for ECHOF. Therefore, we introduced a high-refractive-index salt, LiBr (n = 1.784),[35] to further improve the refractive indices of PAAm hydrogels, as shown in Figure 2b. In this work, we chose 47.6 wt% AAm concentration (relative to the total hydrogel mass excluding LiBr) and 60 wt% LiBr aqueous solution as the solvent for the formation of hydrogel core, which maintains high optical transparency in the visible spectral range (Figure 2c) with a refractive index of 1.472 at 589 nm. The numerical aperture of such step-index optical fiber ($NA = (n_{core}^2 - n_{cladding}^2)^{1/2}$) is 0.413, higher than previously reported hydrogel-based optical fibers.[28, 31] Owing to the finely adjustable refractive index of transparent hydrogel core and the presence of PDMS cladding, light can be efficiently guided in ECHOF (Figure 2d). As measured by a cutback technique, ECHOF possesses a quite low light propagation loss coefficient of ca. 0.32 dB/cm in air, much lower than bare PAAm/LiBr hydrogel optical fiber without cladding (core only, loss coefficient ~0.60 dB/cm) (Figure 2e).

Furthermore, tensile tests show that the maximum elongation of ECHOF is up to 518%, slightly lower than PDMS but higher than hydrogel core (Figure 2f). Since the PDMS cladding is very thin, ECHOF shows a low Young's modulus of ~360 kPa comparable to pure hydrogels, which is small enough for the occurrence of tiny deformations. Cyclic tensile tests between 0% and 100% strain for up to 100 cycles reveals excellent deformation recovery of ECHOF (Figure 2g). The large hysteresis loop in the first cycle is probably due to the rupture of unrecoverable chain crosslinks, which becomes narrower and almost unchanged in the

following cycles, in accordance with the good fatigue resistant behavior of tough PAAm hydrogels.[36]

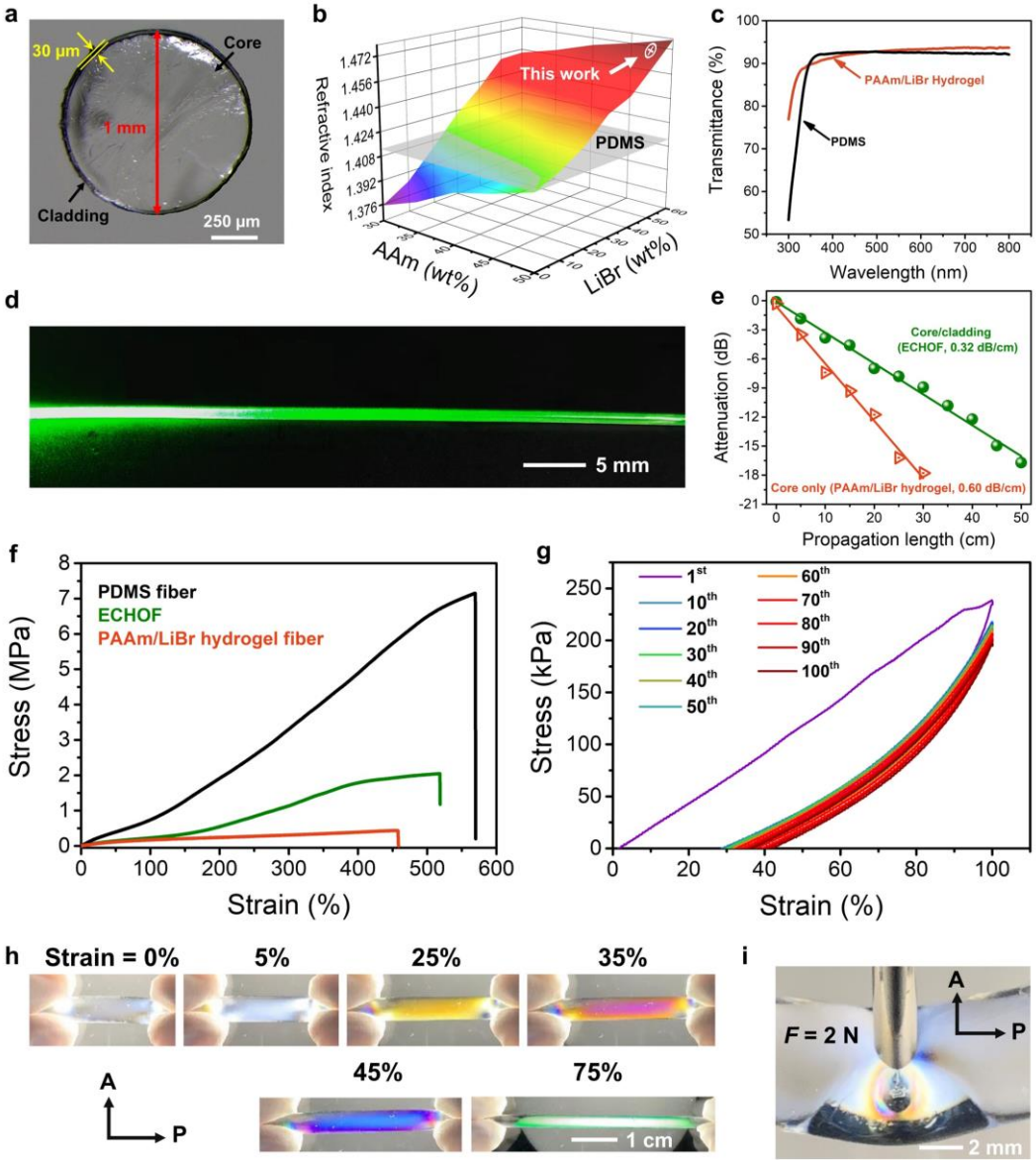

Figure 2. a) Optical microscopic image of the cross-section of a typical ECHOF with an outer diameter of 1 mm and PDMS cladding thickness of ~30 μm. b) The refractive indices (n) of PAAm/LiBr hydrogel as a function of the contents of monomer and LiBr measured at λ = 589 nm. For clarity, the monomer content is relative to the total mass of hydrogel excluding LiBr, while that of LiBr is relative to the concentration of aqueous solution as the solvent. The refractive indices of PDMS (n = 1.413) and PAAm/LiBr hydrogel used in this work (n = 1.472) are also shown. c) UV-vis spectra of PAAm/LiBr hydrogel (500 μm thick) and PDMS (100 μm thick) showing their high optical transparency in the visible spectral range. d) Photo of 532 nm laser light propagation along ECHOF. e) Propagation losses of ECHOF (core/cladding) and bare PAAm/LiBr hydrogel optical fiber (core only) in air, measured by a cutback technique at a laser wavelength of 532 nm. f) Tensile stress-strain curves of ECHOF, PAAm/LiBr hydrogel fiber and PDMS fiber. g) Cyclic stress-strain curves of ECHOF for 100 cycles. h) Strain- and i) compression-induced polarized optical reflection response of ECHOF (outer diameter: 6 mm) demonstrates its readily deformed elastomer-hydrogel interface with internal stress being clearly observed.

The attenuation of an optical fiber measures the total amount of light losses between input and output, including the absorption and scattering of loss elements, macro-/micro-bending losses as well as interface inhomogeneities.[37] In single stretching mode, the principle of strain-induced linear response of attenuation has been well described by Yun et al, which basically follows Beer-Lambert law; that is, as the optical fiber is stretched, the absolute value of optical attenuation (defined as $10\times\lg(I/I_0)$ in a logarithmic (dB) scale; I and I_0 are the output and input intensities, respectively) increases proportionally to the fiber length due to the alteration of loss element distribution in the sensing region (schematic illustration in Figure S5).[28] Moreover, in normal TIR waveguide, as the incident beam is reflected internally at the core-cladding interface with several microns of penetration depth into the cladding layer, the guided wave leakage mainly occurs in the cladding region, as demonstrated by finite element simulation results.[30] Therefore, any kinds of deformation, even very small, could create the local axial distortions of interfacial microscopic curvatures (small-scale bends) that transfer the fundamental mode into higher order non-propagating leaky modes extending into the cladding, resulting in observable optical attenuation.[37] Different from optical fibers with analogous constituting core/cladding materials, ECHOF possesses a much dissimilar hydrogel core and elastomer cladding with distinct Young's moduli (PAAm hydrogel, ~300 kPa; PDMS, ~1.07 MPa) and Poisson's ratios (PAAm hydrogel, ~0.46;[38] PDMS, ~0.50[39]). Such a hybrid whilst adhered structure of ECHOF is anticipated to possess a readily deformed elastomer-hydrogel interface, which is clearly evidenced from its positive and reversible strain- and compression-induced polarized optical reflection response (Figure 2h and i, Movie S2). As a result, high deformation sensing ability reflected by attenuation changes can be expected. Indeed, as demonstrated in the following studies, ECHOF can successfully detect a variety of deformation-based modes like fish lateral lines, including bending, stretching, pressing, hydrostatic pressure, and underwater mechanical waves (acoustic waves and water flows).

First, the transmittance (output light intensity/input light intensity) of ECHOF upon illuminating with a 532 nm laser (power ~4.5 mW) at one end was measured, which shows a monotonic reduction as the other tip of the fiber was bent from 0° to 90° (**Figure 3**a). This bending loss is presumed to arise from both macroscopic curvature-dependent radiation loss and microbending loss caused by the distortion of core-cladding interface.[29] As shown in Figure 3b, the strain sensing properties of ECHOF well follow the linear relation with no apparent hysteresis in one stretching-releasing cycle with progressive strains (0%, 20%, 40%, 60%, 80%, 100%). Furthermore, upon switching the strain between 0% and 100% for 1000 cycles, the attenuation changes of ECHOF are highly repeatable with a long-term high precision (relative standard deviation, RSD ~0.13%) at the maximum strain (Figure 3c, real-time data in Figure S6), indicating the ultrastable performance for sensing strain deformations.

Pressing or indentation is another common type of motions that would induce the local bending or deformation of optical fibers. Upon applying a constant tiny force of 100 mN repeatably with a small indenter (about 265 μm in diameter) onto the fiber for 1000 cycles, the optical response of ECHOF is basically unchanged in the multiple cyclic loading tests with very high stability (RSD ~0.22%) and no obvious mechanical relaxation (Figure 3d, real-time data in Figure S7). The absolute attenuation value increases with the force applied, suggesting the high sensing resolution of ECHOF to gentle pressing (Figure 3e). To further illustrate the high sensitivity of ECHOF, we touched the fiber gently with a finger (<10 kPa), and the fiber sensor could respond very positively (Figure S8).

Since the cladding of ECHOF is a water-proof elastomer, the interference from various underwater medium environments can be greatly reduced as tested in deionized, acidic, alkaline and saline water (Figure S9). Therefore, stable underwater movement sensing that may include the complex deformations of bending, stretching and pressing, becomes possible through ECHOF. For demonstration, we fixed the elastic ECHOF on an electric fish which moves forward freely by swinging its tail. Interestingly, the distinct movement states of fish

tails such as rapid swinging with low amplitudes or slow swinging with large amplitudes can be real-time monitored from the attenuation changes of ECHOF (Figure 3f). In addition, ECHOF is found to be extremely sensitive to hydrostatic pressure depending on the depth for measurement (hydrostatic pressure, $P = \rho gh$; ρ, density of water; g, gravitational acceleration; h, depth) (Figure 3g and Figure S10). A higher hydrostatic pressure further compresses the fiber from all directions that would induce the microdeformation (reduction in size) of ECHOF,[40] leading to a larger light loss. To the best of our knowledge, this is the first report for sensing such subtle hydrostatic pressure changes via stretchable optical sensors.

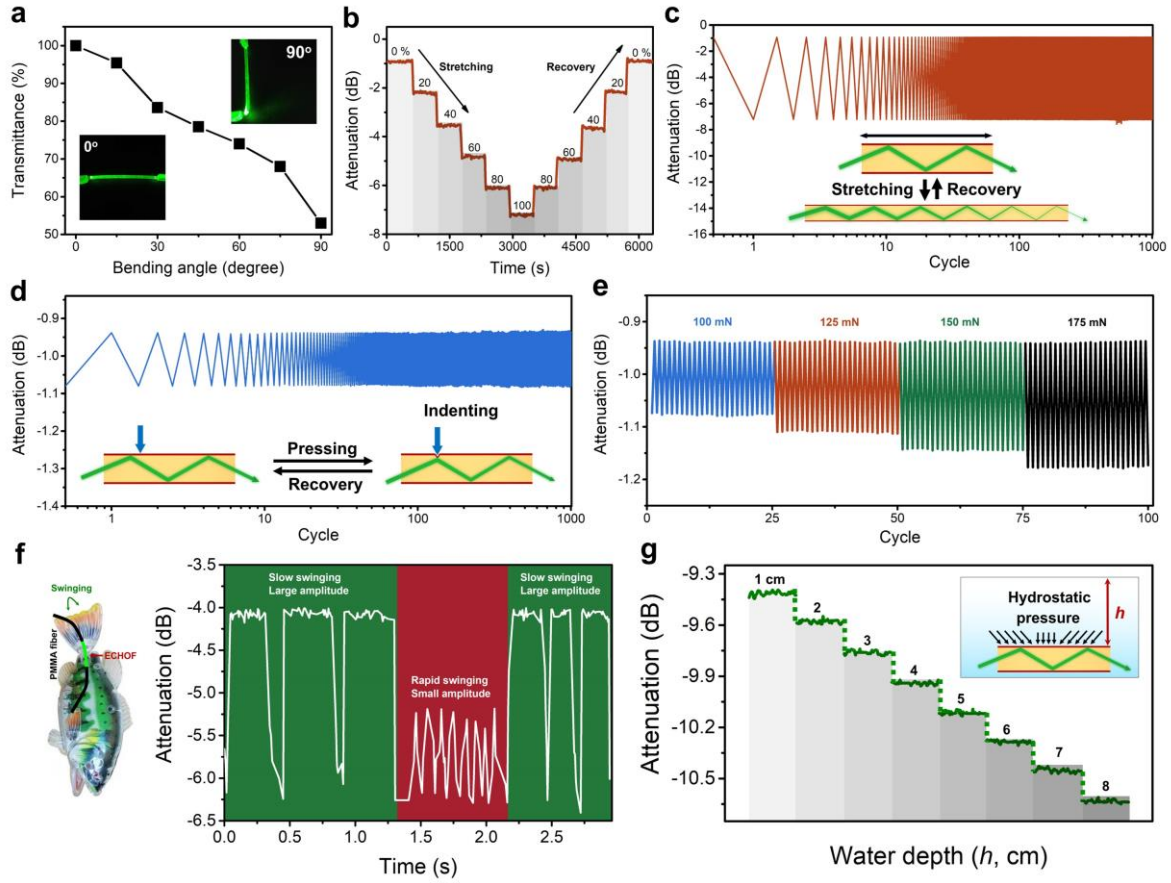

Figure 3. a) Macroscopic bending losses of ECHOF as a function of bending angles. b) The optical attenuation changes of ECHOF upon stretching and releasing with progressive strains of 0%, 20%, 40%, 60%, 80% and 100%. c and d) Attenuation changes of ECHOF by switching strain between 0% and 100% and by cyclic pressing (100 mN) for 1000 cycles, respectively. Schematic light propagation as the fiber is deformed is also shown. e) Attenuation changes of ECHOF by applying gentle indentation forces (100, 125, 150, 175 mN) for 25 cycles each. f) Real-time attenuation changes of ECHOF fixed on a swinging electric fish reflect the fish's movements with different rates and amplitudes. g) The attenuation of ECHOF varies at different water depths (h = 1, 2, 3, …, 8 cm), indicating the sensitive response to hydrostatic pressure.

Analogous to the function of fish lateral line, ECHOF is also able to detect the subtle intermittent water perturbations caused by mechanical waves like acoustic waves and water flows. Acoustic waves are generally longitudinal waves with the same direction of vibration as propagation that result from a pressure oscillation. Therefore, by responding to flow pressure changes around, soft ECHOFs could transfer their own instant microbending/microdeformation to optical signal changes. Here, two kinds of acoustic wave patterns, ultrasonic wave and audible wave, were generated to test the sensing ability of ECHOF (**Figure 4**a). As shown in Figure 4b, switching ultrasonic wave (frequency ~40 kHz, power ~100 W) on and off repeatably leads to obvious real-time response of ECHOF in water. It is noted that, in the case of ultrasonication, ultrasonic cavitation effect[41] may also contribute to the light loss of ECHOF: tiny bubbles created by ultrasonication would vibrate and grow under the action of ultrasonic field, and when the energy reaches a certain threshold, the bubbles collapse and burst, inducing enhanced and fluctuated light scattering of loss elements in the fiber. The audible waves were generated by an underwater loudspeaker which played different letters or phrases, like “Ke”, “A”, “En” and “I have a dream”. It is found that the collected optical signals have a synchronous response to audio waves, and could retain almost every characteristic peak (Figure 4c). The amplitudes of attenuation changes largely depend on the volume of loud. The higher the volume, the stronger the water vibration is, and the larger deformations of ECHOF could be expected to occur with higher light losses (Figure S11).

What’s more, the external perturbations, even gently, may cause water to ripple, and different kinds of perturbations can create water waves with different shapes. The ECHOFs are extremely soft so that they also show an active response to water flow perturbations. The experiment was done as follows: we first placed ECHOF at a depth of 1 cm under water, and another set of water was injected from a syringe needle with the flow direction parallel or perpendicular to the horizonal plane ($\theta = 0^o$ or 90^o), producing annular and vortex flows,

respectively (Figure 4d). Both the two flows diffuse about 1 cm to reach the fiber; however, annular flow diffuses from the center to the outside with flow velocity being gradually reduced, while the flow velocity of vortex wave does not change much (Movie S3). Hence, the attenuation changes of ECHOF caused by a vortex flow are higher than that caused by annular flow with the same distances to the flow source (i.e. syringe needle tip) (Figure 4e).

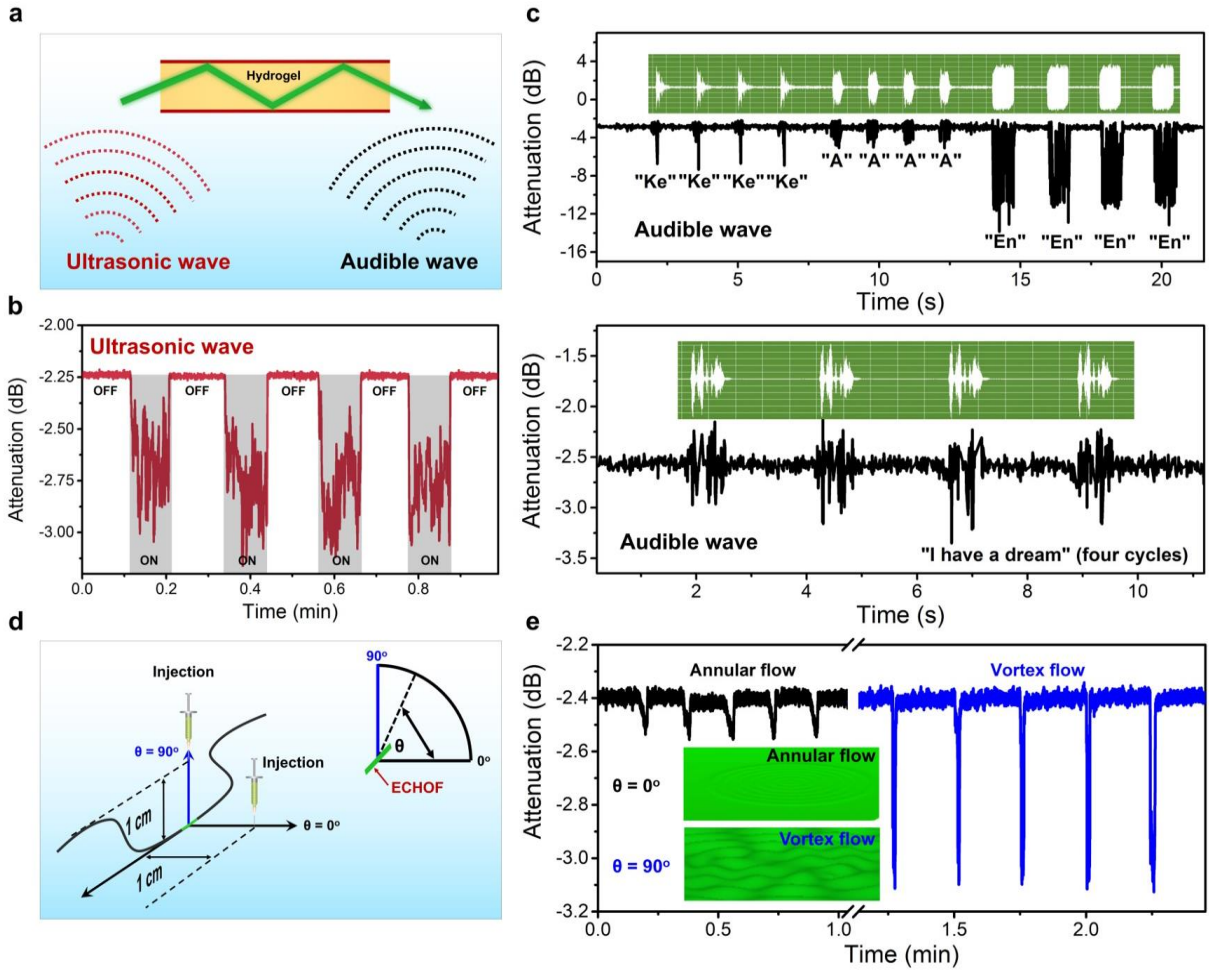

Figure 4. a) Schematic diagram of ECHOF for ultrasonic and audible wave sensing. b) Real-time attenuation changes of ECHOF upon switching ultrasonication on and off. c) Real-time attenuation changes of ECHOF for sensing different audible sound waves. The insets are corresponding input sound signals. (d) Schematic diagram of ECHOF for water flow sensing. Different injection angles generate different flow waveforms ($\theta = 0^o$, annular flow; $\theta = 90^o$, vortex flow). e) Real-time attenuation changes of ECHOF as different waveforms of water flows are applied repeatedly.

Moreover, we further show that the optical losses of ECHOF are also highly sensitive to water temperature variations in a totally non-deformation mode, which is another important

function of fish lateral line. As shown in **Figure 5**a, as temperature rises, the absolute attenuation values of ECHOF decrease almost linearly with high sensitivity (gauge factor, S = 44 mdB $^{o}C^{-1}$ or 3.2% $^{o}C^{-1}$), which is higher than most soft electrical sensors.[42-46] Such a linear relationship enables ECHOF with good capacity to monitor minute-by-minute water temperature changes. For example, we poured hot water to a water bath with ECHOF at intervals and recorded the real-time optical data and water temperature changes with a commercial thermocouple (schematic design in Figure 5b). It is surprising to find that the optical losses of ECHOF could fully reflect the real-time temperature changes of water batch (Figure 5c). Moreover, as LiBr aqueous solution is commonly used in low-temperature absorption chilling, it is expected that ECHOF should also have good anti-freezing properties to be used at subzero temperatures. Indeed, ECHOF still maintains its stretchability as the temperature is lowered to -20 ^{o}C (Figure S12), which can fully meet its uses in the ocean sea (minimum temperature is ca. -1.94 ^{o}C at the sea bottom).

It should be noted that the temperature responsiveness of stretchable optical sensors is rare so far. Pure PDMS optical fiber or common polymer optical fibers like PMMA have no response of optical losses to temperature (Figure S13), unless further functionalized by temperature-sensitive additives.[47] Thus, in the case of ECHOF, the temperature responsiveness may mainly come from the hydrogel core. To elucidate this phenomenon, we performed small-angle X-ray scattering (SAXS) measurements of PAAm/LiBr hydrogel at 30 ^{o}C and 70 ^{o}C, respectively (Figure 5d). The SAXS results of PAAm/LiBr hydrogel could be divided into two regimes (see experimental for fitting details), in which the cluster feature at low q and typical polymer chain scattering at high q are the dominant features respectively. As temperature increases from 30 ^{o}C to 70 ^{o}C, the low q intensity becomes stronger pointing to the formation and growth of clusters. The power law exponent (n) increases from 3.8 to 4 indicating the formation of compact clusters or large aggregates. At the high q regime, the Lorentzian scattering exponent (m) decreases from 1.8 to 1.3 indicating a structural transition

from Gaussian-like chains to rigid chains. The correlation length (ξ) increases from 1.7 nm (30 °C) to 3.2 nm (70 °C) implying that short-range correlations are getting longer. This is probably due to the growth of larger clusters which reduces the number density of free PAAm hydrogel chains.

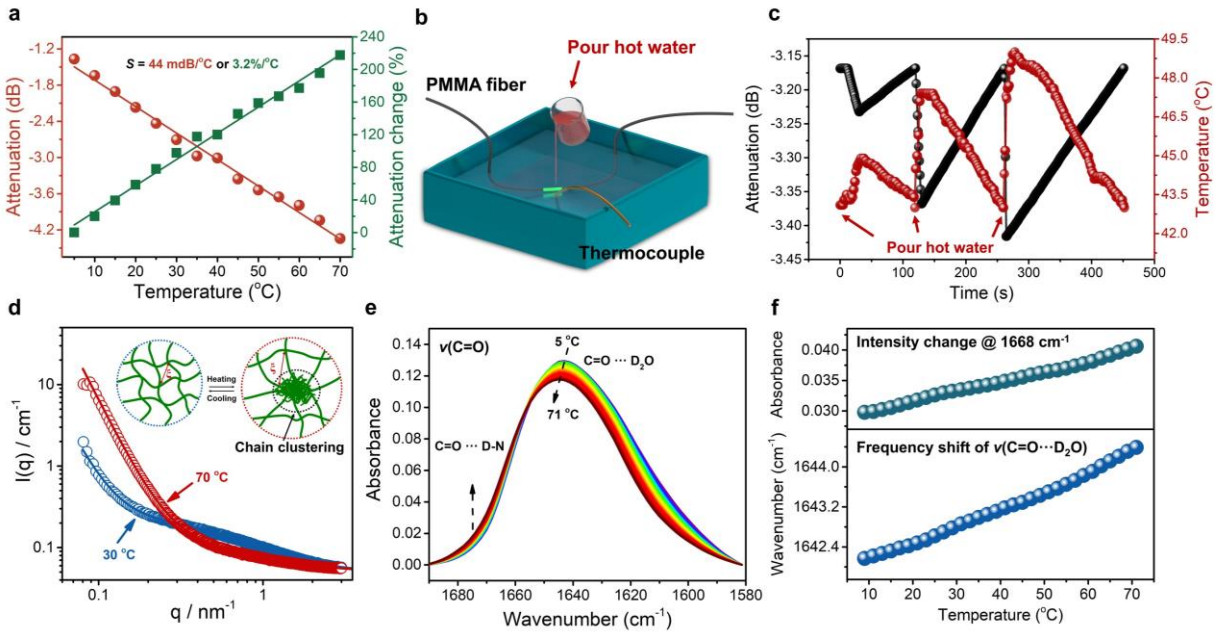

Figure 5. a) The attenuation changes of ECHOF as a function of temperature changes. The linear fitting gives a gauge factor of 44 mdB $^{o}C^{-1}$ or 3.2% $^{o}C^{-1}$. b) Schematic diagram for monitoring water temperature changes by pouring hot water at intervals. c) Real-time attenuation changes of ECHOF and corresponding temperature variations of water bath. d) SAXS scattering intensity I(q) vs q plots of PAAm/LiBr hydrogel at 30 and 70 °C (open circles). The solid lines are the best fitting results using the correlation length model. Schematic chain clustering with increased correlation length (ξ) is also presented. e) Temperature-variable FTIR spectra of PAAm/LiBr hydrogel (solvent: D_2O) during heating from 5 to 71 °C. f) Temperature-dependent wavenumber shifts of ν(C=O···D_2O) around 1642 cm^{-1} and spectral intensity variations of ν(C=O···D-N) at 1668 cm^{-1}.

The formation of larger polymer chain clusters in PAAm/LiBr hydrogel during heating is also evidenced from temperature-variable FTIR spectra at the molecular level (5-71 °C, Figure 5e). We used D_2O instead of H_2O to eliminate the spectral overlapping of ν(C=O) with δ(O-H) of H_2O. The ν(C=O) of PAAm can be roughly considered to the combination of two bands around 1642 and 1668 cm^{-1} assigned to C=O···D_2O and C=O···D-N hydrogen bonds, respectively.[48, 49] The apparent binary changes of ν(C=O) during heating reveal the gradual collapsing of PAAm chains accompanied by the transformation from C=O···D_2O hydrogen

bonds to self-associated C=O···D-N hydrogen bonds. Interestingly, the spectral intensity increase of *v*(C=O···D-N) at 1668 cm^{-1} and frequency shift of *v*(C=O···D_2O) to higher wavenumbers (corresponding to the weakening of hydrogen bonds) are also linearly correlated to temperature changes (Figure 5f), consistent with the macroscopic linear optical sense of ECHOF. Therefore, judging from SAXS and FTIR results, it is clear that the linear temperature response of ECHOF should arise from the gradual formation of larger chain clusters via the self-association of PAAm chains, which inevitably increases the inhomogeneity of hydrogel core.[50] The newly formed more compact clusters possess a higher refractive index than surrounding hydrogel matrix, and thus act as effective loss elements to scatter input light outside, resulting in the increased attenuation of ECHOF. Notably, such clustering effect is rapid and fully reversible in heat-cooling cycles, endowing ECHOF with good durability.

Altogether, despite with a different structure, we have demonstrated that ECHOF can detect very the same stimulations to fish lateral lines for ultrastable underwater sensing in either deformation or non-deformation modes, as shown by all the above descriptions. Such high sensitivity, sensing stability as well as multifunctional underwater sensations of ECHOFs are surprisingly realized by a very simple and easily assembled structure, i.e. elastomer coated hydrogel core. We ascribe these advantages to the following structural features. First, owing to its hydrophobic nature with a low surface energy,[51] the silicone elastomer cladding is ultrathin, but enough to hinder the transportation of most water-permeable substances to alter the optical properties of hydrogel core. Second, the addition of large amounts of LiBr not only brings excellent anti-freezing properties of ECHOF, but also significantly increases the refractive index of hydrogel core, resulting in a high numerical aperture allowing for efficient long-range light propagation. Third, the low Young's modulus and readily distorted hydrogel-elastomer interface of ECHOF make microbending/microdeformation easily take place, which contributes to detectable guided light leakage into the cladding layer, leading to the high

sensitivity of optical sensing. Fourth, the high elasticity of hydrogel core and elastomer cladding as well as their tight interfacial adhesion allow deformations fully recoverable, which explains the unprecedented stability of the hybrid optical fiber. Finally, the gradual and reversible chain network clustering of hydrogel core during heating efficiently changes the distribution of scattering elements, endowing ECHOF with a linear response to water temperature changes in a wide range. Owing to these structural benefits, the present ECHOF in this work exhibits many outstanding sensing characteristics superior to all the previously reported stretchable elastomer or hydrogel-based optical fiber sensors,[18, 19, 21, 22, 28-32, 47, 52] in particular for underwater environments in terms of underwater stability, ultrasonic wave, audible wave, water flow, movement, hydrostatic pressure and temperature sensing (see rough comparison in Table S1).

In summary, inspired by the multiple underwater sensory functions of fish lateral lines, here we report a highly stretchable, step-index elastomer coated hydrogel optical fiber that is capable to perceive a variety of hydrodynamic stimuli with unprecedented sensing stability, including deformation-based bending, stretching, pressing, hydrostatic pressure, acoustic waves, and water flows, as well as water temperature changes. In our design, the introduction of high-refractive-index LiBr to the hydrogel core guarantees effective light propagation via total internal reflection, and the tight adhesion between thin elastomer layer and hydrogel layer renders the optical fiber with both inherent softness and high anti-interference against water-permeable masses. Moreover, the gradual yet reversible hydrogel chain clustering effect during heating is elucidated, which brings almost linear temperature sensitivity in a wide range (5-70 ^{o}C). Although it remains challenging for ECHOF to discern similar attenuation changes originating from the combination of several stimulations as fishes do, this may be solved in the future by cross-correlation processing of optical signals or by integrating several fibers together with controlling stimulating variables (for instance, contact-induced deformations can be largely inhibited by increasing cladding thickness to allow for non-

contact detection only). Notwithstanding, we believe that our proposed elastomer coated hydrogel strategy may inspire more designs of stretchable and stable optical sensors with versatile sensations to be used in a variety of wearable underwater scenarios.

Experimental Section

Fabrication of Elastic PDMS Tubes: PDMS precursors (Dow Corning Sylgard 184, monomer/curing agent = 10:1) were mixed and injected into an acrylonitrile-butadiene-styrene (ABS) tube mold (inner diameter: 1 mm) through a syringe. Then the tube mold was vertically placed for the precursor to level, followed by thermo-curing at 80°C for 40 min. Afterwards, acetone was used to dissolve ABS template and the elastic PDMS tube with a typical thickness of 30 μm can be obtained. The PDMS tube was thoroughly cleaned with methanol and deionized water, and completely dried with nitrogen gas before use. See schematic procedure in Figure S1.

Fabrication of ECHOF: The adhesion between PDMS and hydrogel was achieved by a modified benzophenone strategy.[33, 34] In brief, the inner surface of PDMS tube was first treated by injecting 15 wt% benzophenone solution in ethyl acetate for 1 h at room temperature. Then, the elastomer tube was washed with methanol four times and completely dried with nitrogen gas. The precursor for the hydrogel core was prepared by dissolving 47.6 wt% acrylamide (AAm; Sigma-Aldrich), 0.07 wt% *N*, *N*-methylenebisacrylamide (MBAA; Sigma-Aldrich), and 0.03 wt% 2,2'-azobis(2-methylpropionamidine) dihydrochloride (V50; Sigma-Aldrich) in 60 wt% lithium bromide aqueous solution (the concentrations of monomer, crosslinker and initiator are all relative to the aqueous solution without LiBr). The hydrogel precursor was injected in the benzophenone-treated PDMS tube and then polymerized along with elastomer-hydrogel covalent bonding under ultraviolet irradiation (365 nm) for 1 h at room temperature. As a control sample, pure PAAm/LiBr hydrogel optical fiber without any cladding was also prepared (diameter ~1 mm).

Refractive Index Determination of PDMS and PAAm/LiBr Hydrogels: The refractive indices of PAAm and PAAm/LiBr hydrogels were measured at room temperature using a digital refractometer (PAL-RI; ATAGO) with a built-in yellow light source (589 nm). For measurement, ca. 200 μL of hydrogel precursor was placed on the prism of refractometer and the refractive index was recorded after polymerization under UV irradiation. The refractive index of PDMS was measured from a PDMS film on silicon wafer with an ellipsometer (M-2000UI; J.A. Woollam).

Polarized optical reflection response of ECHOF: The ECHOF was placed in the middle of two polarizers (polarization angle = 90^o) with a white light source below. As the fiber was stretched or pressed, the images were taken on a stereoscopic microscope (Olympus SZX7).

Optical Analysis of ECHOF: Green laser light at 532 nm (CPS532; Thorlabs; typical output power = 4.5 mW) was coupled into ECHOF with a PMMA optical fiber and the output light power was guided out of another PMMA optical fiber and measured by a power meter (PM100D; Thorlabs) equipped with a standard photodiode power sensor (S120VC). To guarantee the close coupling between ECHOF and PMMA optical fiber, the PMMA optical fibers were tightly wrapped by the retained hollow PDMS ends of ECHOF (~0.5 cm long) and fixed with 3M VHB tape. The attenuation of ECHOF was calculated by the equation: $A = 10\times\lg(I/I_0)$, where I and I_0 are the output and input light power, respectively. The propagation losses of bare PAAm/LiBr hydrogel fiber and ECHOF in air were measured by a cutback technique with an interval of 5 cm. The cyclic stretching and indentation of ECHOF for real-time monitoring of light losses were controlled by a universal testing machine (UTM2103; SUNS, Shenzhen, China) and a motorized tension/compression test stand (ESM303; MARK-10). For bending loss tests, one end of the fiber was fixed, and the output light intensity was collected as the fiber was bent from 0^o to 90^o. For electric fish movement measurements, ECHOF was fixed on the linking part of fish tail with two tapes, and then the electric fish was

put into water for real-time optical monitoring. Fish tail swinging can induce the effective deformations of ECHOF with different speeds and amplitudes.

Underwater Sensing of ECHOF for Hydrostatic Pressure, Acoustic Wave, Water Flow and Temperature: For hydrostatic pressure sensing, the ECHOF was fixed on the bottom of a water bath, and the water depth was controlled by adding water to gradually raise water level. The audible sound waves were generated by an underwater loudspeaker, and water flow with different waveforms were produced by injecting water with a syringe needle at different positions of water bath (inject rate: 0.5 mL/s; schematic design in Figure 4d). Ultrasonic waves were generated by an ultrasonic cleaner (~40 kHz, 100 W, KQ2200E). Real-time water temperature changes were controlled by pouring hot water into water bath at intervals and the bath was naturally cooled.

Small-Angle X-ray Scattering (SAXS): SAXS experiments were performed at the Shanghai Synchrotron Radiation Facility (SSRF) beamline BL16B at an X-ray energy of 10.0 keV which corresponds to a wavelength of λ = 1.24 Å. Samples were measured in a liquid cell with two Kapton thin film windows. The sample-detector distance is 1.98 m to cover the scattering vector q range from 0.08 to 4.5 nm^{-1} (q is the scattering vector, $q = (4\pi/\lambda)\sin(\theta)$; 2θ, scattering angle). The scattering patterns were obtained with a short exposure time of 180 s. 60 wt% LiBr solution as the background was subtracted for calculation. The SAXS patterns were radially averaged to obtain the intensity-q profiles. The scattering from PAAm chains and their clustering effect are well described by the empirical correlation length model developed by B. Hammouda et al:[53]

$$\frac{d\Sigma(Q)}{d\Omega} = \frac{A}{Q^n} + \frac{C}{1+(Q\xi)^m} + BK \quad (1)$$

In this equation, the scattering of polymer network is described by the first term A/Q^n and is qualitatively similar to Porod-like scattering that is usually used to evaluate the clustering strength of primary scattering objects. Scattering at larger *Q* is expressed by the second term

$C/[1 + (Q\xi)^m]$ which has been used to characterize the polymer/solvent interaction and chain solvation characteristics. The correlation length ξ represents a weighted average of inter-distances between PAAm chains, and in this paper, ξ identifies the PAAm chain morphology and nanoscopic structure. The amplitudes of Porod and Lorentzian terms (A and C, respectively), and the Porod and Lorentzian scattering exponents (n and m, respectively) were obtained by a nonlinear least-square fitting of the data.

Other Characterizations: All the tensile and peeling stress-strain curves were collected in a universal testing machine (UTM2103; SUNS, Shenzhen, China) at the speed of 10 mm/min. The transmittance of PAAm/LiBr hydrogel and PDMS was recorded on a UV-VIS-NIR spectrometer (Lambda 950; PerkinElmer). Temperature-variable FTIR spectra were collected on an infrared spectrometer (Nicolet iS50; Thermo Scientific) in the transmission mode. For sample preparation, a PAAm/LiBr hydrogel sheet (~0.5 mm thick) was freeze-dried and then swelled in deuterated water at room temperature for three days. The swollen hydrogel sheet was sealed between two ZnSe tablets for FTIR measurement.

Supporting Information

Supporting Information is available from the Wiley Online Library or from the author.

Acknowledgements

We gratefully acknowledge the financial support from the National Science Foundation of China (NSFC) (Nos. 51873035, 21991123) and "Qimingxing Plan" (19QA1400200). We also thank the staffs from BL16B beamline at Shanghai Synchrotron Radiation Facility, for assistance during data collection.

Received: ((will be filled in by the editorial staff))
Revised: ((will be filled in by the editorial staff))
Published online: ((will be filled in by the editorial staff))

References

[1] A. R. Studart, *Angew. Chem. Int. Ed.* **2015**, *54*, 3400.
[2] Y. Yang, J. Chen, J. Engel, S. Pandya, N. Chen, C. Tucker, S. Coombs, D. L. Jones, C. Liu, *PNAS* **2006**, *103*, 18891.
[3] S. Peleshanko, M. D. Julian, M. Ornatska, M. E. McConney, M. C. LeMieux, N. Chen, C. Tucker, Y. Yang, C. Liu, J. A. C. Humphrey, V. V. Tsukruk, *Adv. Mater.* **2007**, *19*, 2903.
[4] M. Krieg, K. Nelson, K. Mohseni, *Nat. Mach. Intell.* **2019**, *1*, 216.
[5] G. Marra, C. Clivati, R. Luckett, A. Tampellini, J. Kronjäger, L. Wright, A. Mura, F. Levi, S. Robinson, A. Xuereb, B. Baptie, D. Calonico, *Science* **2018**, *361*, 486.
[6] N. J. Lindsey, T. C. Dawe, J. B. Ajo-Franklin, *Science* **2019**, *366*, 1103.
[7] M. Kolle, S. Lee, *Adv. Mater.* **2018**, *30*, 1702669
[8] B. Wang, A. Facchetti, *Adv. Mater.* **2019**, *31*, e1901408.
[9] Y. Gao, J. Song, S. Li, C. Elowsky, Y. Zhou, S. Ducharme, Y. M. Chen, Q. Zhou, L. Tan, *Nat. Commun.* **2016**, *7*, 12316.
[10] S. F. Shaikh, H. F. Mazo-Mantilla, N. Qaiser, S. M. Khan, J. M. Nassar, N. R. Geraldi, C. M. Duarte, M. M. Hussain, *Small* **2019**, *15*, 1804385.
[11] X. Su, H. Li, X. Lai, Z. Chen, X. Zeng, *Adv. Funct. Mater.* **2019**, *29*, 1900554.
[12] S. Lin, X. Zhao, X. Jiang, A. Wu, H. Ding, Y. Zhong, J. Li, J. Pan, B. Liu, H. Zhu, *Small* **2019**, *15*, 1900848.
[13] Y. Zou, P. Tan, B. Shi, H. Ouyang, D. Jiang, Z. Liu, H. Li, M. Yu, C. Wang, X. Qu, L. Zhao, Y. Fan, Z. L. Wang, Z. Li, *Nat. Commun.* **2019**, *10*, 2695.
[14] M. Khatib, O. Zohar, W. Saliba, S. Srebnik, H. Haick, *Adv. Funct. Mater.* **2020**, 1910196.
[15] M. Qin, M. Sun, R. Bai, Y. Mao, X. Qian, D. Sikka, Y. Zhao, H. J. Qi, Z. Suo, X. He, *Adv. Mater.* **2018**, *30*, 1800468.
[16] D. Y. Kim, S. Choi, H. Cho, J. Y. Sun, *Adv. Mater.* **2019**, *31*, e1804080.
[17] Y. Wang, W. Niu, C.-Y. Lo, Y. Zhao, X. He, G. Zhang, S. Wu, B. Ju, S. Zhang, *Adv. Funct. Mater.* **2020**, *30*, 2000356.
[18] J. Guo, M. Niu, C. Yang, *Optica* **2017**, *4*, 1285.
[19] C. K. Harnett, H. Zhao, R. F. Shepherd, *Adv. Mater. Technol.* **2017**, *2*, 1700087.
[20] Y. Qu, T. Nguyen-Dang, A. G. Page, W. Yan, T. Das Gupta, G. M. Rotaru, R. M. Rossi, V. D. Favrod, N. Bartolomei, F. Sorin, *Adv. Mater.* **2018**, *30*, 1707251.
[21] A. Leber, B. Cholst, J. Sandt, N. Vogel, M. Kolle, *Adv. Funct. Mater.* **2019**, *29*, 1802629.
[22] D. Shan, C. Zhang, S. Kalaba, N. Mehta, G. B. Kim, Z. Liu, J. Yang, *Biomaterials* **2017**, *143*, 142.
[23] A. S. Kuenstler, H. Kim, R. C. Hayward, *Adv. Mater.* **2019**, *31*, 1901216.
[24] H. Yuk, B. Lu, X. Zhao, *Chem. Soc. Rev.* **2019**, *48*, 1642.
[25] X. Liu, J. Liu, S. Lin, X. Zhao, *Mater. Today* **2020**, DOI: 10.1016/j.mattod.2019.12.026.
[26] M. Choi, J. W. Choi, S. Kim, S. Nizamoglu, S. K. Hahn, S. H. Yun, *Nat. Photonics* **2013**, *7*, 987.
[27] M. Choi, M. Humar, S. Kim, S. H. Yun, *Adv. Mater.* **2015**, *27*, 4081.
[28] J. Guo, X. Liu, N. Jiang, A. K. Yetisen, H. Yuk, C. Yang, A. Khademhosseini, X. Zhao, S.-H. Yun, *Adv. Mater.* **2016**, *28*, 10244.
[29] A. K. Yetisen, N. Jiang, A. Fallahi, Y. Montelongo, G. U. Ruiz-Esparza, A. Tamayol, Y. S. Zhang, I. Mahmood, S.-A. Yang, K. S. Kim, H. Butt, A. Khademhosseini, S.-H. Yun, *Adv. Mater.* **2017**, *29*, 1606380.
[30] N. Jiang, R. Ahmed, A. A. Rifat, J. Guo, Y. Yin, Y. Montelongo, H. Butt, A. K. Yetisen, *Adv. Opt. Mater.* **2018**, *6*, 1701118.
[31] L. Wang, C. Zhong, D. Ke, F. Ye, J. Tu, L. Wang, Y. Lu, *Adv. Opt. Mater.* **2018**, *6*, 1800427.

[32] L. Zhao, J. Gan, T. Xia, L. Jiang, J. Zhang, Y. Cui, G. Qian, Z. Yang, *J. Mater. Chem. C* **2019**, *7*, 897.
[33] H. Yuk, T. Zhang, G. A. Parada, X. Liu, X. Zhao, *Nat. Commun.* **2016**, *7*, 12028.
[34] Y. Lee, S. H. Cha, Y.-W. Kim, D. Choi, J.-Y. Sun, *Nat. Commun.* **2018**, *9*, 1804.
[35] H. H. Li, *J. Phys. Chem. Ref. Data* **1976**, *5*, 329.
[36] R. Bai, Q. Yang, J. Tang, X. P. Morelle, J. Vlassak, Z. Suo, *Extreme Mech. Lett.* **2017**, *15*, 91.
[37] https://www.fiberoptics4sale.com/blogs/archive-posts/95048006-optical-fiber-loss-and-attenuation
[38] T. Takigawa, Y. Morino, K. Urayama, T. Masuda, *Polym. Gels Networks* **1996**, *4*, 1.
[39] R. H. Pritchard, P. Lava, D. Debruyne, E. M. Terentjev, *Soft Matter* **2013**, *9*, 6037.
[40] Y. Wang, S. Gong, S. J. Wang, G. P. Simon, W. Cheng, *Mater. Horiz.* **2016**, *3*, 208.
[41] X. Wang, X. Yu, X. Wang, M. Qi, J. Pan, Q. Wang, *Nano Lett.* **2019**, *19*, 2251.
[42] S. Harada, K. Kanao, Y. Yamamoto, T. Arie, S. Akita, K. Takei, *ACS Nano* **2014**, *8*, 12851.
[43] T. Q. Trung, S. Ramasundaram, B.-U. Hwang, N.-E. Lee, *Adv. Mater.* **2016**, *28*, 502.
[44] S. Y. Hong, Y. H. Lee, H. Park, S. W. Jin, Y. R. Jeong, J. Yun, I. You, G. Zi, J. S. Ha, *Adv. Mater.* **2016**, *28*, 930.
[45] G. Ge, Y. Lu, X. Qu, W. Zhao, Y. Ren, W. Wang, Q. Wang, W. Huang, X. Dong, *ACS Nano* **2020**, 14, 218.
[46] Z. Cao, Y. Yang, Y. Zheng, W. Wu, F. Xu, R. Wang, J. Sun, *J. Mater. Chem. A* **2019**, *7*, 25314.
[47] J. Guo, B. Zhou, C. Yang, Q. Dai, L. Kong, *Adv. Funct. Mater.* **2019**, *29*, 1902898.
[48] B. Sun, Y. Lin, P. Wu, H. W. Siesler, *Macromolecules* **2008**, *41*, 1512.
[49] S. Sun, P. Wu, *Macromolecules* **2010**, *43*, 9501.
[50] S. Seiffert, *Polym. Chem.* **2017**, *8*, 4472.
[51] M. P. Wolf, G. B. Salieb-Beugelaar, P. Hunziker, *Prog. Polym. Sci.* **2018**, *83*, 97.
[52] J. Guo, B. Zhou, R. Zong, L. Pan, X. Li, X. Yu, C. Yang, L. Kong, Q. Dai, *ACS Appl. Mater. Interfaces* **2019**, *11*, 33589.
[53] B. Hammouda, D. L. Ho, S. Kline, *Macromolecules* **2004**, *37*, 6932.

For table of contents entry

Inspired by the multiple sensory functions of fish lateral lines to perceive a variety of hydrodynamic stimuli, a well-defined, highly stretchable, and step-index hydrogel-elastomer hybrid optical fiber (ECHOF) is designed. Owing to the merits of easy deformation, readily distorted hydrogel-elastomer interface, as well as temperature-induced hydrogel chain clustering, ECHOF can mimic nearly all the underwater sensations of fish lateral lines with high sensing stability.

Keyword: Underwater sensing

Chengmin Wang, Baohu Wu, Shengtong Sun*, Peiyi Wu*

Interface Deformable, Thermally Sensitive Hydrogel-Elastomer Hybrid Fiber for Versatile Underwater Sensing